IOP PUBLISHING
IOP FTC
JOURNAL OF PHYSICS D: APPLIED PHYSICS
J. Phys. D: Appl. Phys. **41** (2008) 202007 (5pp)
doi:10.1088/0022-3727/41/20/202007

## FAST TRACK COMMUNICATION

# The effect of the magnetic field strength on the sheath region of a dc magnetron discharge

**E Bultinck and A Bogaerts**

Research Group PLASMANT, Department of Chemistry, University of Antwerp, Universiteitsplein 1, 2610 Antwerp, Belgium

E-mail: evi.bultinck@ua.ac.be

Received 10 July 2008, in final form 29 August 2008
Published 1 October 2008
Online at stacks.iop.org/JPhysD/41/202007

**Abstract**
A 2d3v particle-in-cell/Monte Carlo collisions model was applied to study the influence of the magnetic field strength on the cathode sheath region of a direct current (dc) magnetron discharge. When applying a magnetic field of 520–730 G, the cathode sheath width decreases with magnetic field strength, whereas, if a stronger magnetic field is applied (i.e. from 730 to 2600 G), the sheath width increases. This is explained by studying the structure of the sheath in different magnetic field strengths in terms of the electron and ion densities. The consequences of sheath structure on the sputter deposition process are also investigated. It is found that the magnetic field strength can control the erosion profile and the sputter rate.

(Some figures in this article are in colour only in the electronic version)

The cathode sheath region is the most important area of the magnetron discharge for the sputter process, because it accelerates the ions towards the cathode target, which cause sputtering of the target. Consequently, its structure will undoubtfully influence the sputter deposition process. Therefore, a good understanding is necessary in order to optimize the applications of magnetron sputter deposition.

In spite of its importance, the sheath is also the most complicated and uncomprehended area in (magnetron) discharges. Because of the difference in mobility between electrons and positive ions, the walls charge negatively, creating a positively charged bulk plasma. The region in front of the wall is called the sheath, and is characterized by a decreasing potential from the plasma to the wall. The sheath consists of three different regions [1], i.e. the electron-free ion sheath, the Debye sheath where the electron density rises but stays lower than the ion density, and the pre-sheath, which consists of equal electron and ion densities, but the potential decreases towards the sheath so the ions can accelerate to reach the Bohm velocity [1]. The magnetic field strength determines the structure of the sheath area, but there is uncertainty about which part of the sheath is affected by magnetic field variations [2]. In this study the sheath with all its regions is visualized through the charged particle densities and the potential distribution.

Several authors have studied the sheath behaviour in magnetic fields of different strengths, both experimentally [3–6] and computationally [7–12]. However, the exact reasons for the sheath behaviour are not entirely clarified, especially in the case of high applied magnetic field strengths [2]. Plasma simulation, such as fluid and particle modelling, can be applied to get a better insight in the sheath structure. However, the applied fluid models that study the magnetic field effect use certain assumptions [9, 10]. On the other hand, the existing particle models do not cover the whole magnetic field range but only describe the case of low magnetic fields [7, 8]. Moreover, these particle-in-cell/Monte Carlo collisions (PIC/MCC) models do not include a so-called ‘external circuit’, which occurs to be inevitable for an accurate and correct description of magnetron discharges [13]. Also, sputtering is not accounted for in [7, 8]. Therefore, in this work, the cathode sheath structure and its dependence on

 

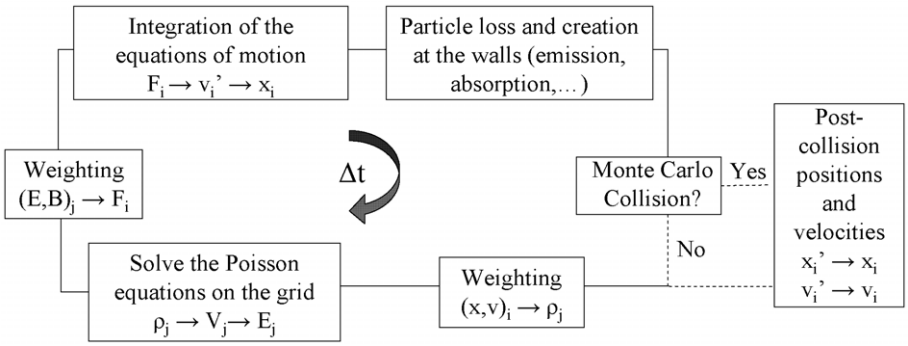


**Figure 1.** Flow chart of the PIC/MCC model. The subscript i denotes the particle quantities and j denotes the grid quantities. (Reused with permission from [13]. Copyright 2008, American Institute of Physics.)

the magnetic field is studied using a 2d3v PIC/MCC model, including an external circuit and the sputter process. This allows us to gain additional insight in the underlying physical mechanisms of the sheath area and all of its regions.

In the 2d3v PIC/MCC model, the real plasma species (i.e. electrons, $Ar^+$ ions, metastable Ar atoms, fast Ar atoms, $Ti^+$ ions and fast Ti atoms) are presented as a limited ensemble of superparticles (SPs). Their movement is described by Newton's laws. Their collisions, given in [14] (but Cu is replaced by Ti), are treated probabilistically with the Monte Carlo method. Their interactions with the walls are also accounted for, such as the sputtering of the Ti target (characterized by the sputter yield from Matsunami [15]), ion- or atom-induced secondary electron emission, electron reflection, heavy particle reflection, neutralization and de-excitation. The Poisson equation is solved to calculate the electrical potential distribution, including hereby an external circuit, as described in [13]. The flow chart of the model is given in figure 1, and further details of this method are given in [13, 14, 16–19].

The magnetron under study is a planar circular balanced magnetron, as presented in [13, 20]. The magnetron operates in a pure argon gas at 300 K, at a pressure of 1 Pa, and a titanium cathode target is sputtered. The plasma current and potential are calculated self-consistently.

A magnetic field distribution, with maximum radial magnetic field strength of 1040 G at the target surface and at a radial position of $r = 13.5$ mm, was provided by Mahieu [21]. In order to study the influence of the magnetic field strength, the $B_r$ and $B_z$ values of this magnetic field are multiplied by factors of 0.5, 0.55, 0.6, 0.7, 1.5 and 2.5, leading to maximum radial field strengths of 520 G, 570 G, 620 G, 730 G, 1560 G and 2600 G, respectively. Due to this applied non-uniform magnetic field, the particle densities in the plasma will have a non-uniform distribution. Therefore, the sheath will also be non-uniform, being thinnest at the maximum radial magnetic field. The term 'sheath width' refers to the point where the plasma is the most intense and the sheath the thinnest, i.e. above the race track.

The normalized plasma potential distribution on the line above the race track (i.e. $r = 13.5$ mm) for the different magnetic field strengths is presented in figure 2. For the weaker applied magnetic fields, i.e. in this case from 520 to 730 G, the

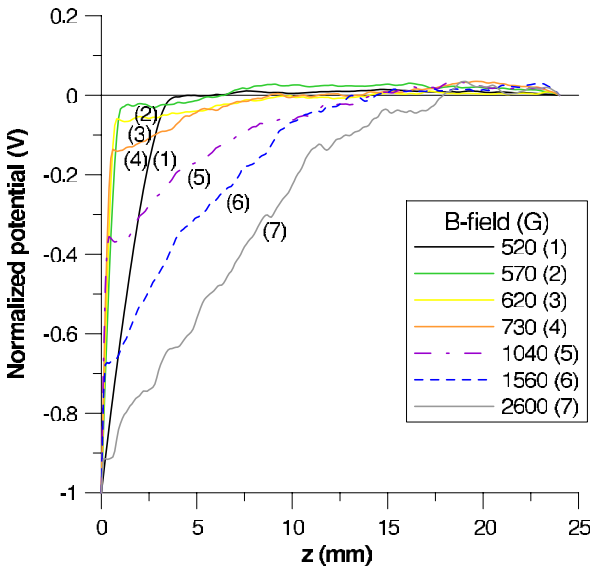


**Figure 2.** (Colour online) Normalized calculated potential distribution at a line above the race track (i.e. $r = 13.5$ mm), for different values of the magnetic field, as indicated in the legend.

sheath thickness decreases when the magnetic field strength is increased. Similar results of a decreasing sheath width were found experimentally by Kuwahara *et al* [3], for an increase in the magnetic field strength from 10 to 190 G, by Bowden *et al* [4], when increasing the magnetic field strength from 200 to 450 G, and by Gu *et al* [5] when increasing the magnetic field from 140 to 570 G. Computational studies also confirm this contraction of the sheath: Kondo *et al* [7] calculated a decrease in sheath thickness when increasing the magnetic field from 330 to 660 G, Nanbu *et al* [8] when increasing the magnetic field from 250 to 1000 G and Bradley *et al* [10] when increasing the magnetic field strength from 30 to 110 G. Pandey *et al* [12] studied the effect of separate electron and ion magnetization and found a decrease in sheath width with increasing magnetization, albeit, for larger magnetic field variations.

Since the sheath structure is determined by the ion distribution, the ion densities on the same line above the race track are presented in figure 3. Only the $Ar^+$ ion density is presented, since this is the dominant ion, determining the potential distribution. At low applied magnetic field

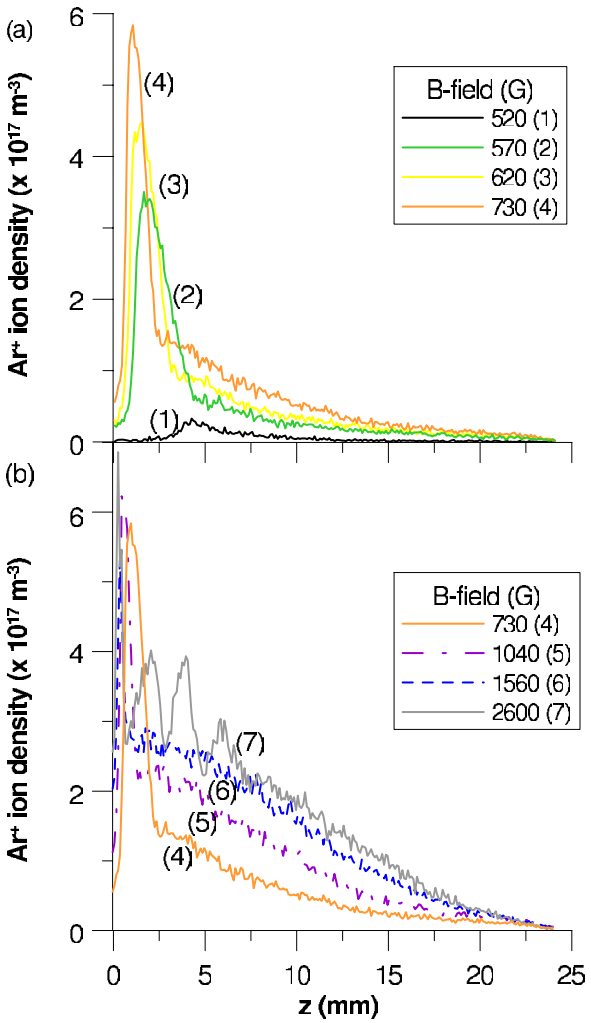


**Figure 3.** (Colour online) Calculated $Ar^+$ densities at a line above the race track (i.e. $r = 13.5$ mm), for low (*a*) and high (*b*) magnetic field strengths.

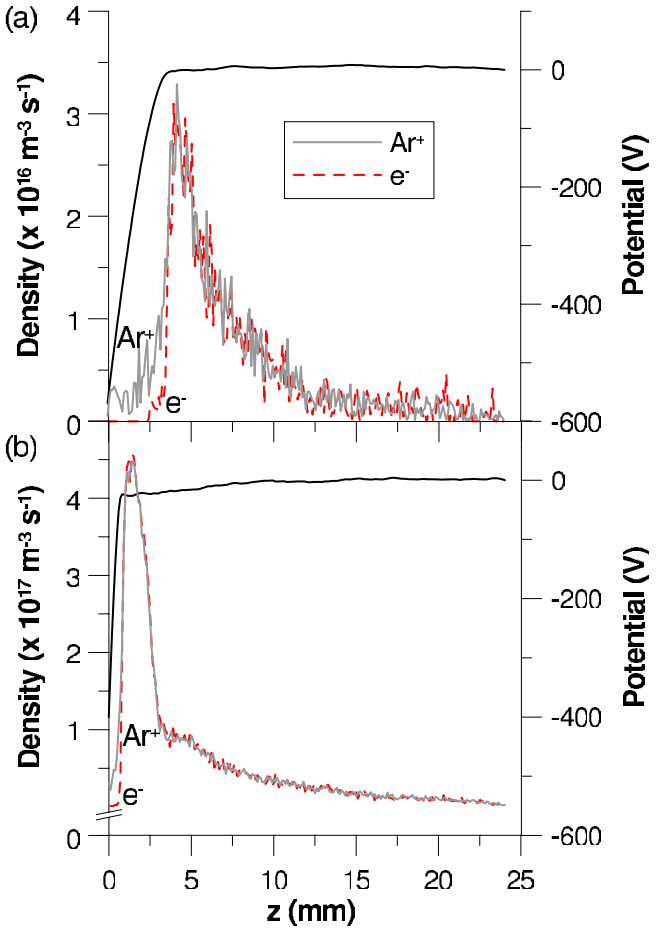


**Figure 4.** (Colour online) Calculated electron (dashed line) and $Ar^+$ (solid line) densities, and potential distribution at a line above the race track (i.e. $r = 13.5$ mm), for a magnetic field strength of 520 G (*a*) and 620 G (*b*). For better visualizing, the *y*-axis in (*b*) is stretched out between 0 and $10^{15}$, since the electron density at $z = 0$ mm is $6.5 \times 10^{15}$ m$^{-3}$ s$^{-1}$.

strengths (figure 3(*a*)), a higher density peak is observed with increasing magnetic field, which is shifted towards the cathode, explaining the thinner sheath. The shift towards the cathode is justified by the well-known fact of decreasing Debye length with rising ion density.

Note that for these weak magnetic fields, the profile of the plasma potential (figure 2) is similar to the case of a non-magnetized plasma. However, when a magnetic field is applied of at least 730 G, figure 2 shows a sudden broadening of the potential profile. This broadening becomes more distinct with rising magnetic field strength. Wendt and Lieberman [11] have found evidence for these so-called 'thick sheaths', and measurements of Yeom [6] also confirm this. Lister [9], using a 1D fluid model, finds a broadening of the sheath when increasing the magnetic field as well, in the case of a sufficiently strong magnetic field (up to 1000 G).

The corresponding ion density profiles, presented in figure 3(*b*), show that the peak of the ion densities is approximately constant when increasing the magnetic field (although it shifts slightly towards the cathode), but in the tail of the profile, the ion densities increase. This is explained as follows. The electrons gyrate around the magnetic field lines with their Larmor radius. If the magnetic field is weak, the electrons are easily lost to the cathode wall, causing the creation of a positive ion sheath, figure 4(*a*) (at $z = 0$–2.5 mm). When the magnetic field strength is increased, the Larmor radius becomes smaller, until the electron is virtually trapped in the pre-sheath by the strong magnetic field. Therefore, its movement to the cathode wall is inhibited, leading to a less pronounced potential build-up on the cathode wall and a less pronounced positive space charge in front of the cathode. This so-called magnetized pre-sheath or Chodura layer was also reported in [22–24]. In our case, the electron density in front of the cathode even rises above zero, meaning that the ion sheath disappears. The Debye sheath narrows, and the pre-sheath widens. As a result, it is observed from our calculations that at a certain magnetic field strength (i.e. around 620–730 G, see figure 4(*b*)) the electron density starts to spread out towards the tail of the pre-sheath. Correspondingly, also the ion density expands (i.e. the pre-sheath widens), as presented in figure 3.

It is clear that the difference in sheath behaviour in a weak or a strong magnetic field will influence the sputter process. In a weak magnetic field, the ion density peak

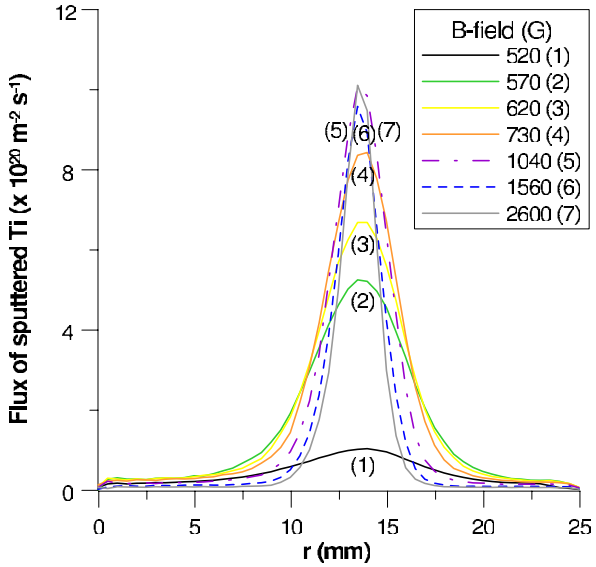


**Figure 5.** (Colour online) Flux of sputtered Ti particles from the cathode target as a function of radial position, for different values of the magnetic field. The sputter flux increases with magnetic field strength for low magnetic field, until it remains constant for high magnetic field (although the profile narrows). For symmetry reasons, only half of the target is shown.

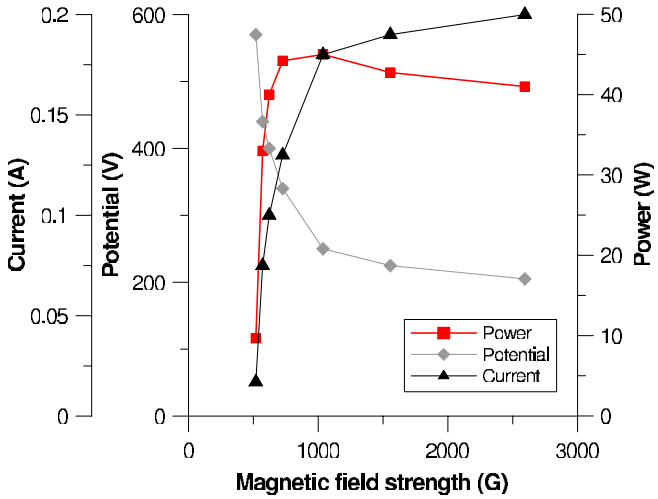


**Figure 6.** (Colour online) Calculated cathode current, (absolute value of the) potential and power, for different values of the magnetic field.

increases with the magnetic field. As a consequence, more Ti particles will be sputtered from the cathode surface, presented in figure 5. On the other hand, when increasing further the magnetic field strength above 730 G, the ion density tail increases but the peak stays constant. Therefore, the amount of sputtering remains approximately constant, as is clear from figure 5. A similar behaviour was also found for the calculated fluxes of the depositing atoms at the substrate (not presented here).

The effect of the magnetic field on the sputter and deposition rates can also be explained by the electrical current, potential and power, which are calculated self-consistently in the model, and are presented in figure 6. With rising magnetic field strength, the current increases and the potential drops (both first significantly, later more slowly). Consequently, the power rises strongly for the low magnetic field strengths, but remains approximately constant at the high magnetic field strengths. This demonstrates that the power is more or less linearly connected to the sputtered Ti flux. This is logical because the sputter flux is determined by (i) the flux of the bombarding ions which is proportional to the current, and (ii) the sputter yield which depends on the voltage [15].

It is worth mentioning that the sputter profile is also strongly influenced by the magnetic field. At low magnetic field strengths, the sputter flux is low but spread out, whereas, for high magnetic field strengths, the flux is high but very narrow. The amount of sputtering determines the erosion of the target. Therefore, at weak magnetic fields, although the sputter flux is low, the target is consumed more efficiently. At strong magnetic fields, there is a high sputter flux, but the erosion profile is very deep and narrow. In other words, the magnetic field is able to control the depth and the width of the erosion profile, and a considered choice of its strength is essential for the optimal balance between a high sputter flux and an efficiently consumed target.

## Acknowledgments

E Bultinck is indebted to the University of Antwerp for financial support. The authors would like to thank M Gaillard, S Mahieu and D Depla for the interesting discussions on the sheath structure and the sputter process, and for providing the magnetic field. The computer facility CALCUA from the University of Antwerp is acknowledged.

## References

[1] Lieberman M A and Lichtenberg A J 1994 *Principles of Plasma Discharges and Materials Processing* (New York: Wiley)
[2] Buyle G 2005 Simplified model for the DC planar magnetron discharge *PhD Thesis* Ghent University
[3] Kuwahara K and Fujiyama H 1994 Applications of the Child–Langmuir law to magnetron discharge plasmas *IEEE Trans. Plasma Sci.* **22** 442
[4] Bowden M D, Takamura T, Muraoka K, Yamagata Y, James B W and Maeda M 1993 Measurements of the cathode sheath in a magnetron sputtering discharge using laser induced fluorescence *J. Appl. Phys.* **73** 3664
[5] Lan Gu and Lieberman M A 1988 Axial distribution of optical emission in a planar magnetron discharge *J. Vac. Sci. Technol.* A **6** 2960
[6] Yeom G Y and Thornton J A 1989 Cylindrical magnetron discharges. Current–voltage characteristics for dc- and rf-driven discharge sources *J. Appl. Phys.* **65** 3816
[7] Kondo S and Nanbu K 1999 A self-consistent numerical analysis of a planar dc magnetron discharge by the particle-in-cell/Monte Carlo method *J. Phys. D: Appl. Phys.* **32** 1142
[8] Nanbu K and Kondo S 1997 Analysis of three-dimensional dc magnetron discharge by the particle-in-cell/Monte Carlo method *Japan. J. Appl. Phys.* **36** 4808
[9] Lister G 1996 Influence of electron diffusion on the cathode sheath of a magnetron discharge *J. Vac. Sci. Technol.* A **14** 2736

[10] Bradley J W and Lister G 1997 Model of the cathode fall region in magnetron discharges *Plasma Sources Sci. Technol.* **6** 524
[11] Wendt A E and Lieberman M A 1990 Spatial structure of a planar magnetron discharge *J. Vac. Sci. Technol.* A **8** 902
[12] Pandey B P, Samarian A and Vladimirov S V 2007 Dust in the magnetized sheath *Phys. Plasmas* **14** 093703
[13] Bultinck E, Kolev I, Bogaerts A and Depla D 2007 The importance of an external circuit in a particle-in-cell/Monte Carlo collisions model for a direct current planar magnetron *J. Appl. Phys.* **103** 013309
[14] Kolev I and Bogaerts A 2006 Detailed numerical investigation of a dc sputter magnetron *IEEE Trans. Plasma Sci.* **34** 886
[15] Matsunami N, Yamamura Y, Itikawa Y, Itoh N, Kazumata Y, Miyagawa S, Morita K, Shimizu R and Tawara H 1984 Energy dependence of the ion-induced sputtering yields of monatomic solids *At. Data Nucl. Data* **31** 1
[16] Birdsall C K and Langdon A B 1991 *Plasma Physics via Computer Simulations* (Bristol: Institute of Physics Publishing)
[17] Kolev I and Bogaerts A 2004 Numerical models of the planar magnetron glow discharges *Contrib. Plasma Phys.* **44** 582
[18] Kolev I, Bogaerts A and Gijbels R 2005 Influence of electron recapture by the cathode upon the discharge characteristics in dc planar magnetrons *Phys. Rev.* E **72** 056402
[19] Kolev I and Bogaerts A 2006 PIC/MCC numerical simulation of a dc planar magnetron *Plasma Process. Polym.* **3** 127
[20] Depla D, Buyle G, Haemers J and De Gryse R 2006 Discharge voltage measurements during magnetron sputtering *Surf. Coat. Technol.* **200** 4329
[21] Mahieu S Measurements at Ghent University, private communications
[22] Chodura R 1982 Plasma–wall transition in an oblique magnetic field *Phys. Fluids* **25** 1628
[23] Kim G H, Hershkowitz N, Diebold D A and Cho M H 1995 Magnetic and collisional effects on presheaths *Phys. Plasmas* **2** 3222
[24] Singha B, Sarma A and Chutia J 2002 Experimental observation of sheath and magnetic presheath over an oblique metallic plate in the presence of a magnetic field *Phys. Plasmas* **9** 683